Magnetism and NIR dual-response polypyrrole-coated Fe_3O_4 nanoparticles for bacteria removal and inactivation

Na Guo[a,b,c+], Feng Cang[a+], Zhen Wang[a], Ting-Ting Zhao[a], Xin-Rui Song[a], Stefano Farris[c], Yan-Yan Li[a,*] and Yu-Jie Fu[a,*]

[a.] *College of Chemistry, Chemical Engineering and Resource Utilization, Northeast Forestry University, Hexing Road 26, Harbin, 150040, PR China*

[b.] *College of Materials Science and Engineering, Northeast Forestry University, Hexing Road 26, Harbin, 150040, PR China*

[c.] *DeFENS, Department of Food, Environmental and Nutritional Sciences, University of Milan, via Celoria 2, 20133, Milan, Italy*

+ These authors contributed equally to this work.

*Corresponding authors

Email addresses: liyanyan_ls@126.com (Yan-Yan Li), yujie_fu@163.com (Yu-jie Fu) Tel: +86-451-82190535, Fax: +86-451-82190535

Abstract

Microbial contamination of water represents a great threat to the public health that has attracted worldwide attention. In this work, polypyrrole magnetic nanoparticles (Fe_3O_4@PPy NPs) with sterilization properties were fabricated. More specifically, the Fe_3O_4@PPy NPs obtained via aqueous dispersion polymerization and an *in situ* chemical oxidative polymerization exhibited a cationic surface and high photothermal conversion efficiency. Using *E. coli* as a model system, it was possible to observe that more than 50% of bacteria adsorption can be achieved at a dosage of 100 μg/mL under magnetic field, and high photothermal sterilization efficacy (~ 100%) can be obtained upon NIR exposure at the same dosage for 10 min. Noteworthy, the Fe_3O_4@PPy NPs can be recycled by magnetism and reused without affecting their photothermal sterilization capability. This study clearly provides experimental evidence of the great potential of Fe_3O_4@PPy NPs as stable and reusable nanocomposite material for photothermal sterilization applications.

Keywords: bacteria adsorbent; cationic polymers; *E. coli*; photothermal sterilization; water safety management.

43 **Graphical Abstract**

44

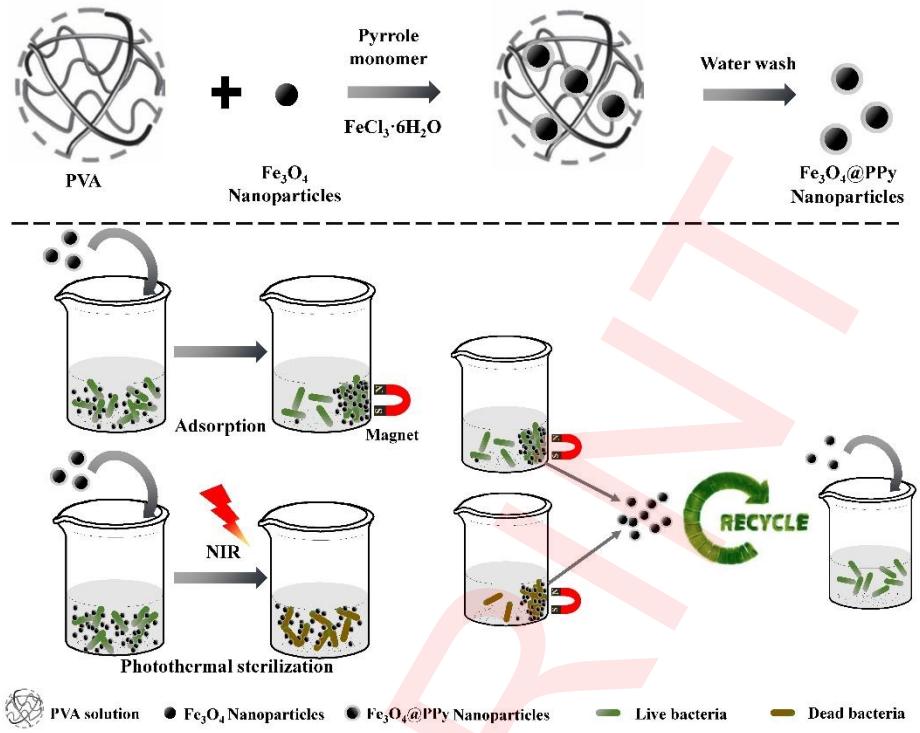

45

1. Introduction

It has been estimated that 80 countries in the world suffer from shortage of drinking water, with approximately 1.2 billion people being exposed to contaminated drinking water.[1] Proliferation of pathogens bacteria has been regarded as one of the main causes of water contamination, which can lead to dysentery, colitis, and even uremia, with a negative impact on the public health and safety.[2] Water safety management is therefore attracting an increasing attention all over the world. Until now, the approaches used to disinfect the contaminated water foresee physical and chemical processes. Physical processes usually include filtration, thermal treatment, and ultraviolet (UV) irradiation. However, these approaches have their shortages and limitations. For example, they are time consuming, bio-resources wasting, and their applications are limited.[3] Chemical processes are based on the use of additives, such as traditional agents (chlorine, chlorine dioxide, ozone, *etc.*)[4] and novel agents (antibiotics, metal particles, *etc.*).[5] However, issues associated to their cost and toxicity make these agents an unfavorable option. For all the above reasons, there is a need to explore more suitable approaches to eliminate bacteria in drinking water in an efficient way.

In the past few years, photothermal transduction agents (PTAs) have obtained widely recognition in cancer therapy, whereby PTAs now represent a promising alternative to conventional approaches.[6] PTAs can harvest energy from light and convert the energy into heat, generating local heat even up to 70 °C.[7] Since most bacteria can be devitalized above 55 °C,[8] photothermal sterilization mediated by PTAs is a viable option for microbial control.[9] Sun *et al.* utilized prussian blue as photothermal agent with excellent

bacterial inactivation performance.[9a] However, prussian blue can rapidly decompose under alkaline conditions, which hinder its use for practical purposes.[10] It is notable that part of the photothermal agents are susceptible to pH, ionic strength, and other adverse environments, which influence the stability and thermal conversion efficiency, beside raising serious concerns on the possible formation of toxic by-products.[11] Therefore, it is of utmost importance to select most suitable photothermal agents in order to achieve an efficient photothermal sterilization of water.

Polypyrrole nanoparticles, a new type of low cost, highly stable, and biocompatible photothermal agents, have received great attention in photothermal therapy.[12] They have been demonstrated as wide-coverage materials, being able to interact efficiently within the entire UV-visible spectrum, up to the near infrared (NIR) region. The low wavelength coverage (UV-light region) is attributed to the $\pi - \pi^*$ transition for the conjugated polypyrrole backbone, whereas the broad wavelength coverage from the visible region to the NIR region is the characteristic of the bipolaronic polypyrrole.[13] Moreover, polypyrrole nanoparticles are also stable in alkaline or acidic surroundings and can bear exposure to severe conditions.[14] Based on these properties, polypyrrole nanoparticles are well suited to utilize a large portion of the solar spectrum for photothermal sterilization.

Magnetic nanoparticles have attracted great interest due to their intrinsic properties.[15] In the field of water management, they can be easily dispersed and recovered from the aqueous medium by on/off switching of an external magnetic field, with great advantage in terms of no losses, no energy consumption, and no by-products

formation.[16] Among the different types of magnetic nanoparticles, Fe_3O_4-based nanoparticles have been widely used for a variety of applications, especially due to their low cost and biocompatibility.[17] Because of the negative charge of the cell membrane of bacteria, using positively-charged magnetic nanoparticles is expected to promote the nanoparticle/bacteria interaction, thus improving the removal efficiency.[18]

In this study, polypyrrole magnetic nanoparticles (Fe_3O_4@PPy NPs) were prepared via aqueous dispersion polymerization and an *in situ* chemical oxidative polymerization method. The proposed nanomaterials have been conceived as an alternative approach for water sterilization in the broad context of water safety management. To this scope, the obtained nanoparticles were characterized in terms of morphology, dispersibility in water, conversion efficiency of the absorbed NIR photons into heat, bacteria removal efficiency, and photothermal sterilization ability. The reusability of Fe_3O_4@PPy NPs was also evaluated.

2. Experimental

2.1. Materials

Ethylene glycol, polyvinyl alcohol (PVA) and pyrrole were purchased from Aladdin chemicals company (Shanghai, China). Iron chloride hexahydrate ($FeCl_3 \cdot 6H_2O$), trisodium citrate and sodium acetate were purchased from Beijing chemical reagents company (Beijing, China). All the chemicals and reagents were of analytical grade. Deionized (DI) water (18.25 MΩ·cm) was acquired from a Milli-Q water-purification system (Bedford, MA, USA).

2.2. Preparation of the Fe_3O_4@PPy NPs

2.2.1. Synthesis of Fe_3O_4 nanoparticles

The Fe_3O_4 nanoparticles (Fe_3O_4 NPs) were prepared via a modified solvothermal reaction as previously reported.[17a] Briefly, 1.3 g $FeCl_3 \cdot 6H_2O$ and 0.40 g trisodium citrate were dissolved in 40 mL ethylene glycol by means of an ultrasonicator (KQ-400KDV, Kunshan, China). Then, 2.4 g sodium acetate was added to the above solution and stirred at 1000 rpm for 30 minutes. The obtained homogeneous solution was sealed in a Teflon-lined stainless-steel autoclave (100 mL volume) and heated at 200 °C for 12 h. After cooling to room temperature, the products were washed three times with ethanol and water, and the final nanoparticles were dried under vacuum for 12 h at 45 °C.

2.2.2. Synthesis of Fe_3O_4@PPy NPs

The Fe_3O_4@PPy NPs were synthesized via an *in situ* chemical oxidative polymerization method in the presence of Fe_3O_4 @NPs. Briefly, 3.0 g PVA was dissolved in 30 mL hot DI water under mechanical agitation until a clear sticky liquid was obtained. After cooling to room temperature, 100 mg of Fe_3O_4 NPs was redispersed in the PVA solution under ultrasonication at room temperature for 10 min. Then, the solution was equilibrated for 1 h before 200 μL of pyrrole monomer was added. After further stirring for 30 min, 1.6 g $FeCl_3 \cdot 6H_2O$ was used as an oxidant to initiate the polymerization. The polymerization proceeded at room temperature for 6 h to obtain Fe_3O_4@PPy NPs. The so obtained nanoparticles were collected by magnetic separation and then washed with hot water for three times to remove pyrrole in excess and other reagents. The final nanoparticles were dried under vacuum for 12 h at 45 °C.

2.3. Characterization

The size and morphology of Fe_3O_4 NPs and Fe_3O_4@PPy NPs were determined by transmission electron microscopy (TEM) (H-7650, Hitachi Instruments, Japan) operating at an acceleration voltage of 100 kV. Thermogravimetric analysis (TGA) was carried out with a thermogravimetric analyzer (449C, TA Instruments, USA) at a heating speed rate of 10 °C/min under N_2 atmosphere from room temperature to 800 °C. Fourier transform infrared (FTIR) spectroscopy was performed using an infrared spectrometer (Nicolet IS 5, Thermo Scientific, USA) with KBr as background over the range of 4000–400 cm^{-1}. The magnetic properties of nanoparticles were assessed using a quantum design system (PPMS-9, Quantum Design Company, USA) at room temperature with a maximum magnetic field of 10 kOe. Hydrodynamic diameter and zeta potential measurements were run by dynamic light scattering (DLS) equipment (ZetaPALS, Brookhaven Instruments, USA). The UV-vis spectra ranging from 400 nm to 900 nm were obtained with a UV-vis spectrophotometer (UV-2600, Shimadzu Instruments, China).

2.4. Photothermal performance of Fe_3O_4@PPy NPs

The photothermal performance of Fe_3O_4@PPy NPs was firstly evaluated by acquiring the real-time photothermal heating curves exposed to NIR laser irradiation (808 nm, 2 W/cm^2). Fe_3O_4@PPy NPs aqueous dispersions at different concentrations (10, 20, 50, 100 μg/mL) were irradiated for 10 min. The temperature change was monitored and recorded every 30 s using a submerged digital thermometer with a thermocouple microprobe. The heating curve was made by plotting the measured temperature versus time. DI water irradiated by NIR laser was used as control. In addition, the effect of radiant power at different levels (0.5, 1, 1.5, 2 and 2.5 W/cm^2 for 10 min exposure) on photothermal performance was also determined. The temperature

change was monitored and recorded every 30 s, and the heating curve was plotted. The photothermal conversion efficiency of Fe_3O_4@PPy NPs was measured by recording the temperature change of dispersion under continuous irradiation of an 808 nm laser (2 W/cm^2) until the temperature of the solution reached a steady-state evolution, followed by spontaneous cooling to room temperature. The photothermal conversion efficiency was calculated according to the calculation method reported by Chang et al.[19] The photostability of Fe_3O_4@PPy NPs was analyzed by the LASER ON and LASER OFF procedure with NIR laser described by Li et al. with a little modification.[20] The LASER ON procedure was operated for 10 min, and then the samples were let to cool to room temperature for 30 min with no exposure to NIR laser irradiation (LASER OFF). This cycle was continuously repeated for 5 times. The real-time temperature increase of Fe_3O_4@PPy NPs upon the NIR laser irradiation (2 W/cm^2) was visualized by IR thermal camera (Ti25, Fluke, USA).

2.5. Bacteria culture and preparation

The *E. coli* strains were used as a model microorganism in this study. They were provided by the Institute of Applied Microbiology, Heilongjiang Academy of Science (China). Bacteria cultures were maintained on an agar plates at 4 °C and subcultured monthly. Before each experiment, *E. coli* were activated in nutrient broth at 37 °C up to the mid-log phase. The bacteria suspensions were centrifuged at 3502 g for 10 min and washed with saline buffer (0.9 wt% NaCl in water). The *E. coli* cells were then poured into a buffer solution to achieve the required concentration.

2.6. Bacteria removal efficiency

Fe_3O_4@PPy NPs at different concentrations were added in 10^6 colony forming unit

(CFU) bacteria suspension (3 mL) and thoroughly dispersed for 10 minutes to promote interaction between NPs and bacteria. An external magnet was then placed on the wall of the cuvette, the NPs set aside by the magnetic field, and the clear suspension separated and collected in a beaker. The removed suspension was diluted appropriately and seeded on agar plates. Thereafter, the CFU of the bacteria suspension was counted by the plate counting method. Briefly, 100 µL of the diluted suspension was placed onto a sterile solid medium and cultured at 37 °C for 24 h. Bare bacteria suspensions (i.e., which did not enter in contact with Fe_3O_4@PPy NPs) were used as a control.

2.7. Photothermal sterilization

Fe_3O_4@PPy NPs at different concentrations were added in 10^6 CFU bacteria suspension (3 mL) and then irradiated with 808 nm wavelength at a power density of 2 W/cm^2 for 10 min. The bacteria suspension without irradiation was used as a control. After irradiation, the suspensions were used for estimating the photothermal sterilization activity of Fe_3O_4@PPy NPs by plate counting method, following the same procedure described above.

2.8. Recyclability

After a first photothermal sterilization test, Fe_3O_4@PPy NPs were collected by a magnetic force for 10 min, and then subjected to a 3 min water bath sonication for removal of impurities. A second photothermal sterilization test was thus performed, up to a total of four cycles. At the end of each cycle, the photothermal sterilization activity of the recycled Fe_3O_4@PPy NPs was determined by plate counting method. The UV-vis spectra of the recycled Fe_3O_4@PPy NPs exposed to NIR irradiation and magnetic

separation were also recorded.

2.9. Bacteria morphology change observation

The interaction between *E. coli* and Fe_3O_4@PPy NPs and the morphological change of *E. coli* after NIR irradiation were observed by TEM. More specifically, the *E. coli*/Fe_3O_4@PPy NP complexes were first collected and the excess (unbound) *E. coli* cells and impurities washed out with DI water. At this point, the interaction between *E. coli* and NPs was evaluated by TEM. The *E. coli* and Fe_3O_4@PPy NPs suspensions after NIR irradiation were centrifuged and washed with DI water for morphological change observations by TEM. The untreated *E. coli* were taken as control.

3. Results and discussion

3.1. Preparation and characterization of Fe_3O_4@PPy NPs

Amongst various magnetic nanoparticles, experimental evidence suggests that those obtained by the modification of carboxylate groups exhibit favorable stability, biocompatibility, and dispersibility.[21] In this study, carboxylate groups-modified magnetite nanoparticles were synthesized via a modified solvothermal reaction. Then, an *in situ* chemical oxidative polymerization method was used to fabricate Fe_3O_4@PPy NPs.

As shown in **Figure 1A** and **Figure 1B**, both Fe_3O_4 NPs and Fe_3O_4@PPy NPs exhibited uniform spherical shape. Compared with Fe_3O_4 NPs, a thin layer coated on the surface of Fe_3O_4@PPy NPs was clearly visible, indicative of the successful modification of the nanoparticles with pyrrole polymers. Particle size measurement by TEM revealed that the mean size of Fe_3O_4 NPs and Fe_3O_4@PPy NPs was 185 ± 15 nm

and 210 ± 23 nm, respectively. The slight size increase for Fe_3O_4@PPy NPs can be attributed to the shell structure of pyrrole polymer. The hydrate particle sizes of Fe_3O_4 NPs and Fe_3O_4@PPy NPs were 216 ± 18 nm and 293 ± 27 nm, respectively (**Figure 1C**). The larger particle size measured by DLS compared to TEM images was due to the fact that the mean diameter of NPs by DLS was calculated from the diffusional properties of dynamic nanoparticles in hydrated state, whereas in the case of TEM images, they were captured from nanoparticles in dried state.[22] The zeta potential of Fe_3O_4 NPs was -16.77 ± 1.40 mV, but it increased up to 15.89 ± 0.87 mV after modification with polypyrrole (**Figure 1D**), which behaved as a positively-charged polymer. Fe_3O_4@PPy NPs exhibited a core–shell architecture, which was attributed to the commonion effect of the oxidant Fe^{3+} aggregated around the surface of Fe_3O_4 NPs and the complexation processes of Fe_3O_4 core with polypyrrole. The common-ion effect and complexation processes ensured the success of the particles preparation, and enhanced the stability of the Fe_3O_4@PPy NPs.[23]

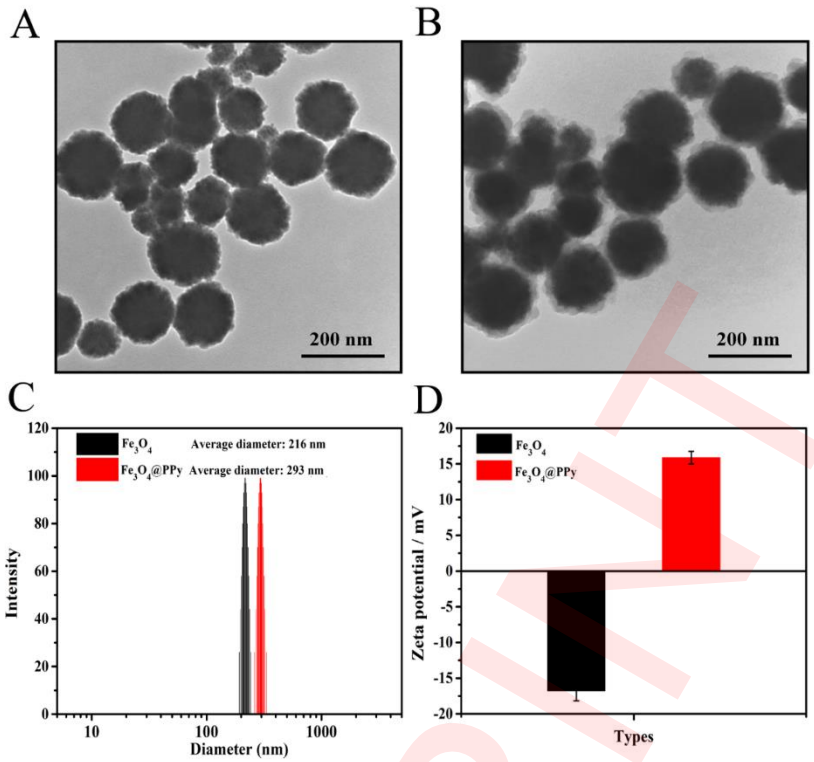

Figure 1. TEM images of Fe_3O_4 NPs (A) and Fe_3O_4@PPy NPs (B), hydrodynamic diameter of Fe_3O_4 NPs and Fe_3O_4@PPy NPs (C), and zeta potential of Fe_3O_4 NPs and Fe_3O_4@PPy NPs (D).

The FT-IR spectroscopy results of the Fe_3O_4 NPs and Fe_3O_4@PPy NPs are shown in **Figure 2A**. For Fe_3O_4 NPs, the bands at 563 and 420 cm^{-1} were both associated with the Fe-O stretching, while the bands centered at 1601 and 1390 cm^{-1} were assigned to the carboxylate group. The bands at 1052 and 3376 cm^{-1} were ascribed to the vibrating mode of both C-H and O-H functional groups.[24] The characteristic absorption bands of Fe_3O_4@PPy NPs at 1556 and 1403 cm^{-1} were attributed to the fundamental stretching vibration of pyrrole rings, whereas the band at 1297 cm^{-1} was attributed to C-N stretching vibration. The other peaks at 1195, 1043, 910 and 786 cm^{-1} were due to the in-plane, out-of-plane, C-H and N-H bending vibrations. The shifting of the peak

associated with the Fe-O stretching from 563 cm^{-1} to 605 cm^{-1} indicates the presence of Fe_3O_4 as well as the interaction of Fe_3O_4 with polypyrrole.[25] All these peaks demonstrated the successful preparation of Fe_3O_4@PPy NPs.

Figure 2B showed the TGA plots of the Fe_3O_4 NPs and Fe_3O_4@PPy NPs. The different stages of weight loss were correspondingly due to different physicochemical degradation phenomena of the nanoparticles. The first weight loss of both Fe_3O_4 NPs and Fe_3O_4@PPy NPs ranging from 64 ℃ to 142 ℃ might be attributed to the loss of adsorbed water. The second weight loss of Fe_3O_4 NPs, ranging from 280 ℃ to 400 ℃, might be possibly generated by the degradation of magnetic nanoparticles. Conversely, the second weight loss (from 260 ℃ to 670 ℃) observed for the Fe_3O_4@PPy NPs might be attributed to the degradation of polypyrrole. Finally, the third weight loss appeared only in the Fe_3O_4@PPy NPs was plausibly due to the degradation of the core part of magnetic nanoparticles.

The magnetic properties of Fe_3O_4 NPs and Fe_3O_4@PPy NPs were determined by the measurement of the magnetic hysteresis curve at 300K (room temperature). As shown in **Figure 2C**, both Fe_3O_4 NPs and Fe_3O_4@PPy NPs had the typical superparamagnetic behavior. At the same time, it was not surprising that the modification of Fe_3O_4 NPs surface with polypyrrole weakened the magnetic properties, due to the nonmagnetic features of polypyrrole. The saturation magnetization value of the Fe_3O_4@PPy NPs was 23.87 emu/g, which was strong enough for magnetic separation.[26] The visual photos of the Fe_3O_4@PPy NPs suspensions before and after the application of an external magnetic field were displayed in the inset of **Figure 2C**. The Fe_3O_4@PPy NPs can be well-dispersed in the aqueous solution without any external magnetic field; when a magnet was placed on the wall of the cuvette, the Fe_3O_4@PPy NPs rapidly moved toward the cuvette wall and the suspension turned from black to totally transparent, thus

confirming that the polypyrrole was tightly bound to the Fe_3O_4 NPs, with virtually no residual (unbound) pyrrole polymer in the solution.

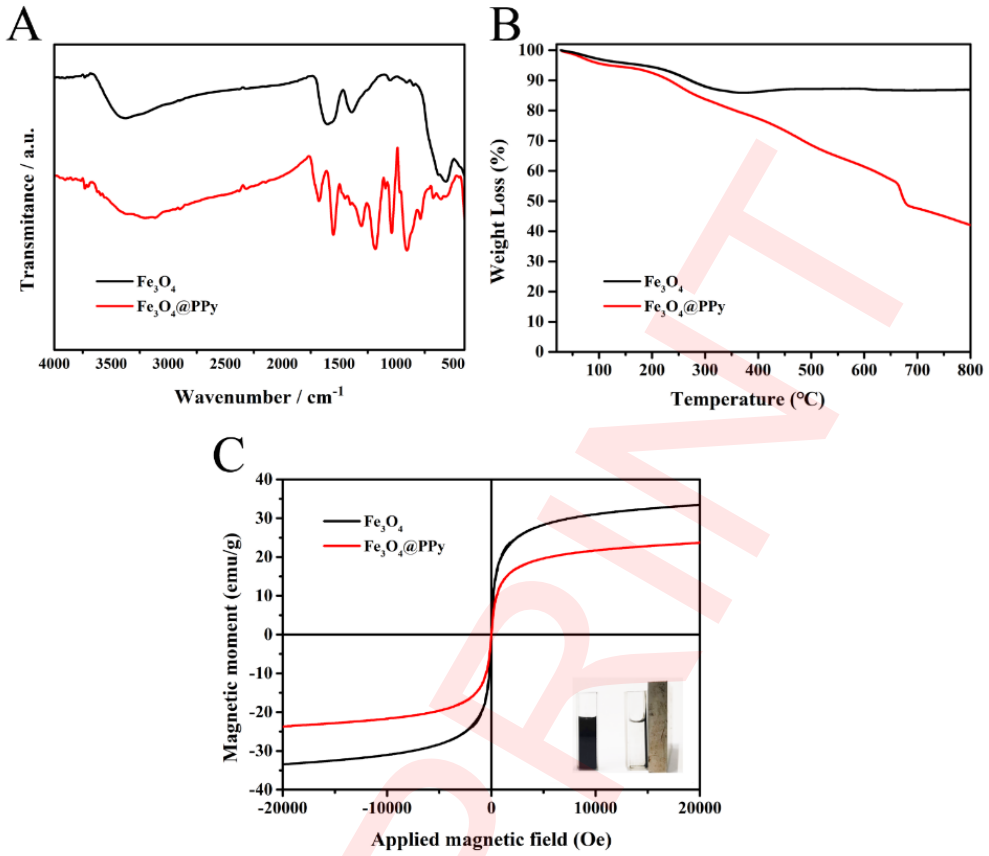

Figure 2. FTIR spectra (A) and TGA curves (B) of Fe_3O_4 NPs and Fe_3O_4@PPy NPs, and magnetic hysteresis curve of the Fe_3O_4 NPs and Fe_3O_4@PPy NPs at 300 K (C). The insert in the figure is the photograph of Fe_3O_4@PPy NPs suspensions before and after an external magnetic field treatment.

An ideal photothermal nanomaterial should have strong spectral absorption and high photothermal conversion ability.[12a] The spectral absorption of Fe_3O_4@PPy NPs was firstly measured by UV-vis spectra. As shown in **Figure 3A**, the Fe_3O_4@PPy NPs possessed a strong and broad absorption in the range from 400 nm to 900 nm, which endowed the Fe_3O_4@PPy NPs with both NIR-driven and full-spectrum applications.

The absorption at 900 nm was the characteristic of the bipolaronic band transitions of pyrrole polymers,[27] and the absorbance of the Fe_3O_4@PPy NPs at 900 nm was in a high level. This demonstrated that the Fe_3O_4@PPy NPs had the properties of polypyrrole, which has potential in photothermal applications.

3.2. Photothermal properties of Fe_3O_4@PPy NPs

To evaluate the photothermal properties of Fe_3O_4@PPy NPs, the photothermal conversion ability was measured under NIR laser exposure (808 nm, 2.0 W/cm^2) by monitoring the real-time temperature changes. As shown in **Figure 3B**, a temperature increase was observed with increasing the concentration of Fe_3O_4@PPy NPs from 10 to 100 μg/mL. Moreover, the temperature increase was also dependent on the power density of the incident NIR light, as shown in **Figure 3C.** In particular, 10 min of NIR laser irradiation of 100 μg/mL Fe_3O_4@PPy NPs solution made possible a temperature increase from 28.9 °C to 60.1 °C. In comparison, the temperature of only water (i.e., in the absence of Fe_3O_4@PPy NPs) upon 808 nm laser for 10 min only had a 2.1 °C increment. Here, the temperature variation of water can be assumed to be negligible compared to the effect observed for the Fe_3O_4@PPy NPs exposed to the same irradiation power density. For the determination of the photothermal conversion efficiency of Fe_3O_4@PPy NPs, we further measured the temperature change under continuous irradiation, until a steady-state temperature level was achieved. At this point, the laser was turned off to record the equilibrium temperature (**Figure 3D**).

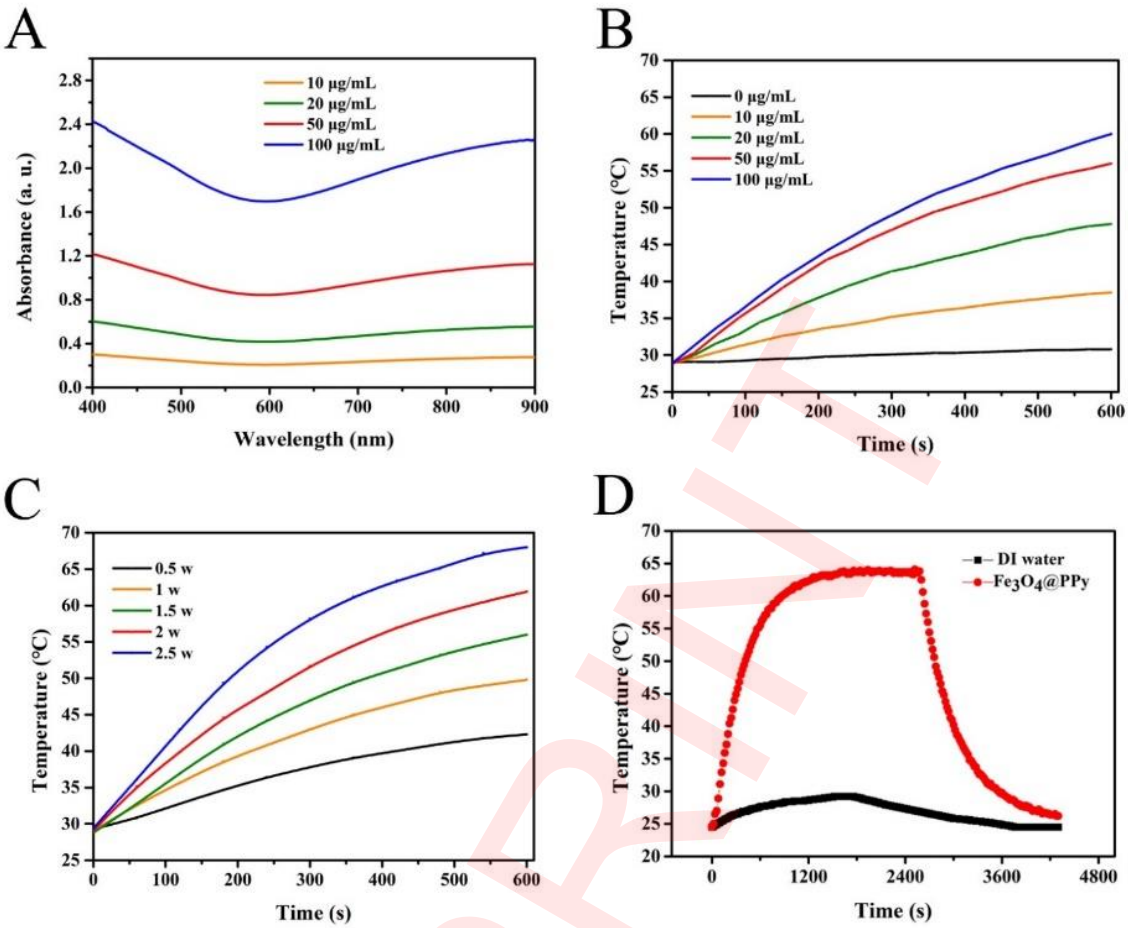

322

323 **Figure 3**. UV-vis spectra of the Fe_3O_4@PPy NPs (A), temperature increase of the
324 different concentrations of Fe_3O_4@PPy NPs (B), temperature changes of the
325 Fe_3O_4@PPy NPs with different laser power densities (C), and photothermal heating
326 curves of the Fe_3O_4@PPy NPs and DI water (D).

327

328 The relationship between cooling time and negative natural logarithm of the
329 temperature driving force is shown in **Figure 4A**. The time constant for the heat transfer
330 of the system was determined to be $\tau s = 484$ s. According to the generated results, the
331 calculated photothermal conversion efficiency of the Fe_3O_4@PPy NPs was 17%. The
332 "on-off" temperature curves of Fe_3O_4@PPy NPs during five cycle examination were
333 presented in **Figure 4B**. The negligible fluctuation in temperature at each irradiation

cycle demonstrated the stability of the photothermal performance of the Fe_3O_4@PPy NPs. The real-time thermal images of Fe_3O_4@PPy NPs exposed to irradiation are shown in **Figure 4C**. The color of the solutions gradually changed from blue (corresponding to low temperature) to dark red (corresponding to high temperature), clearly indicating that the temperature of Fe_3O_4@PPy NPs solution increased with increasing both the irradiation time and sample concentration. These results indicated that the prepared Fe_3O_4@PPy NPs featured high photothermal conversion and good photothermal stability properties, which can be effectively used in photothermal applications.

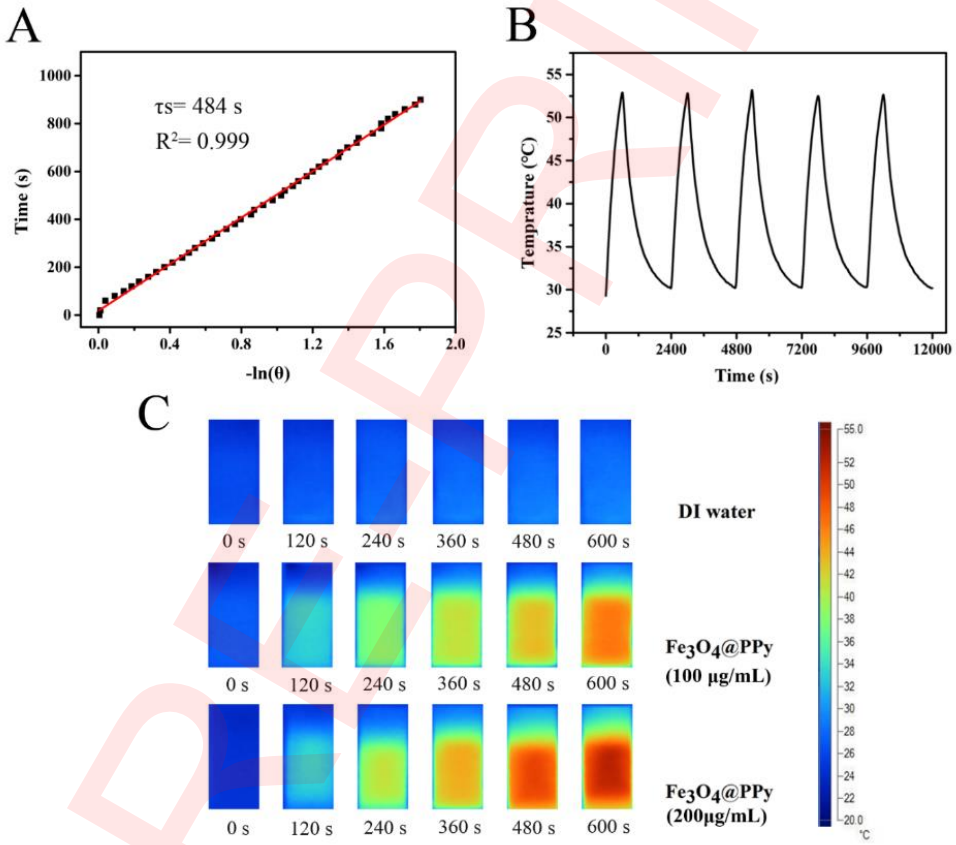

Figure 4. Photothermal conversion efficiency (A) and photostability (B) of Fe_3O_4@PPy NPs and thermal images of DI water and Fe_3O_4@PPy NPs (C).

3.3. Bacteria removal efficiency of Fe_3O_4@PPy NPs

Many approaches have been undertaken in water safety.[3c, 5c, 28] Adsorbent materials, in particular, outperformed the conventional chemical flocculant precipitation and disinfection processes used in water treatment.[29] Magnetic nanoparticles have been regarded as a kind of novel adsorbent materials due to their ease of removal of target species from water with an external magnetic field, high surface area and efficient adsorption capacity. With special reference to bacterial adsorbent materials, the negatively charged molecules on the bacteria cell wall provide anionic sites for electrostatic binding of cationic molecules.[30] According to this principle, cationic magnetic adsorbent materials were fabricated with the purpose to effectively capture and remove bacteria in water systems.[1, 31]

In the present study, *E. coli* was taken as a model microorganism to determine the bacteria removal efficiency of the prepared cationic magnetic nanoparticles (Fe_3O_4@PPy NPs). **Figure 5A** shows the remaining *E. coli* after separation of the Fe_3O_4@PPy NPs/*E. coli* complex with an external magnetic field, whereas the statistical analysis of the bacteria viability was displayed in **Figure 5C**. The decreased bacteria viability demonstrated the increased bacteria removal efficiency with the increase of the Fe_3O_4@PPy NPs concentration. After 10 min of interaction and 10 min of magnetic adsorption, more than 50% *E. coli* was removed at a 100 μg/mL Fe_3O_4@PPy NPs concentration. The *E. coli* removal efficiency was previously tested using magnetic graphene composites. Compared with the pure Fe_3O_4 NPs, the magnetic graphene composites showed better removal performance against *E. coli*, which was mostly attributed to the much larger surface area of the graphene nanoparticles. However, it must be noted that the bacteria removal efficiency was still not effective, because more than 15 min were necessary to achieve an effective removal of the *E.*

coli.[31b] In our study, the simultaneous establishment of electrostatic interactions between the cationic Fe_3O_4@PPy NPs and the peptidoglycans and proteins of the bacteria cell membrane,[30] boosted the aggregation and complex formation between the Fe_3O_4@PPy NPs and *E. coli* cells. In turn, the complex can be easily separated using an external magnetic field, thus enhancing the bacteria removal efficiency.[32] Therefore, the cationic Fe_3O_4@PPy NPs, with the advantages of ease of handling and favorable adsorption performance, can be taken as a promising bacteria adsorbent material.

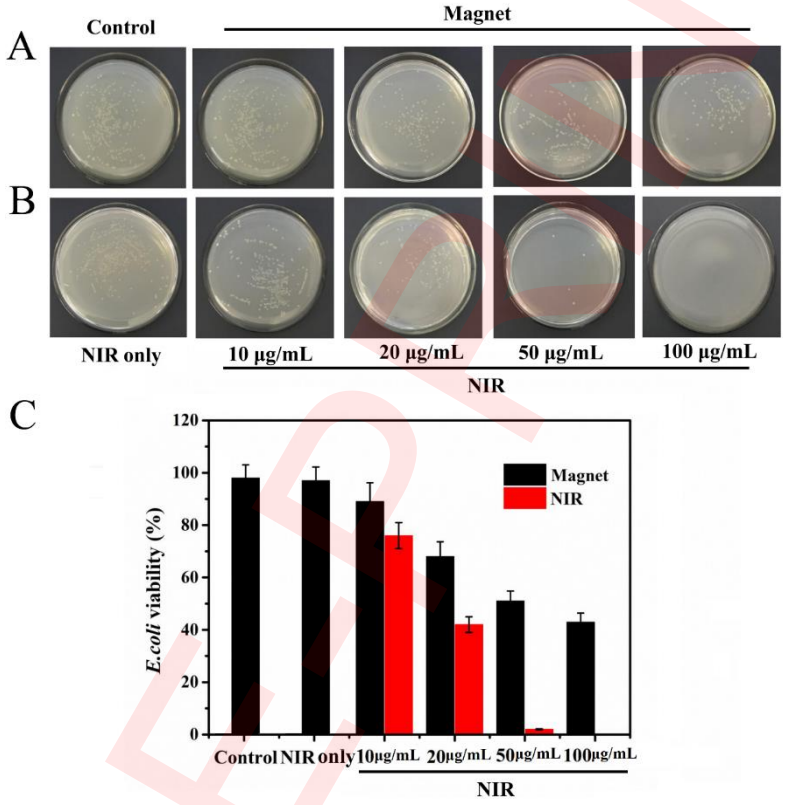

Figure 5. Photographs of residual *E. coli* after magnetic adsorption treatment (A), survival *E. coli* after photothermal treatment (B), and *E. coli* viability (C).

3.4. Photothermal sterilization property of Fe_3O_4@PPy NPs

Based on our previous works, we took on enormous effort to expand the application of the photothermal nanoparticles.[12a, 33] Due to the excellent photothermal performance

of Fe_3O_4@PPy NPs, we further investigated their photothermal sterilization induced by NIR radiation of the electromagnetic spectrum. The survived *E. coli* strains after NIR irradiation is shown in **Figure 5B**, whereas the results in **Figure 5C** demonstrated that the photothermal sterilization performance of Fe_3O_4@PPy NPs increased with increasing NPs concentration. After continuous irradiation for 10 min, 100% of *E. coli* strains were inactivated with a concentration of 100 μg/mL Fe_3O_4@PPy NPs. The sterilization mechanism of Fe_3O_4@PPy NPs was mostly due to the hyperthermia on bacteria. It has been reported that 55 °C was the threshold temperature, above which denaturation of proteins and synthesis of heat-shock proteins would occur. Long-time heat treatments would break the intracellular circulation of bacteria and lead to their death.[34] In the present work, after 10 min NIR irradiation, the temperature of 100 μg/mL Fe_3O_4@PPy NPs rose to 60.1 °C, which was enough to inactivate the bacteria. Arising from these results, as expected Fe_3O_4@PPy NPs exhibited effective photothermal sterilization activity, which can be profitably exploited for the generation of a new class of photothermal sterilization agents against bacteria in aqueous medium.

3.5. Morphology observation of *E. coli* and Fe_3O_4@PPy NPs

TEM images were used to acquire a deep understanding of the interaction between *E. coli* and Fe_3O_4@PPy NPs upon magnetism, as well as the morphology changes of *E. coli* after NIR irradiation (**Figure 6**). *E. coli* cells without any treatment exhibited an intact and smooth morphology (**Figure 6A**). After adding the Fe_3O_4@PPy NPs into the *E. coli* suspension, the Fe_3O_4@PPy NPs adsorbed onto the *E. coli* surface (**Figure 6B**). The morphology of the *E. coli* was damaged severely after NIR irradiation, as confirmed by the shrinkage of the bacteria cytoplasm followed by rupture of the cell wall and membrane (**Figure 6C**).

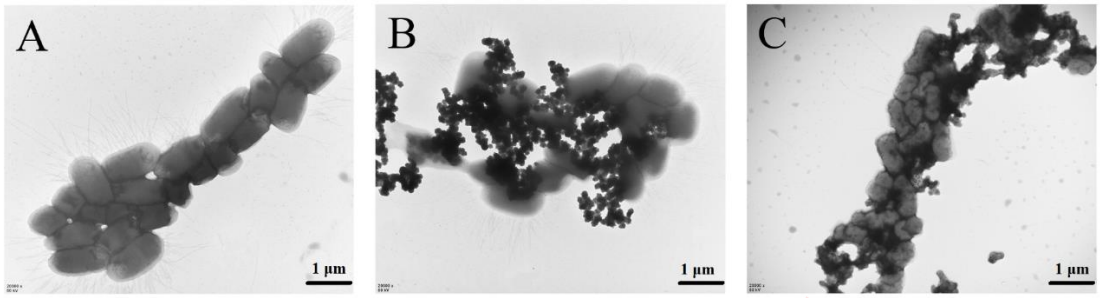

Figure 6. TEM images of *E. coli* cells (A), *E. coli* cells and Fe_3O_4@PPy NPs treated with an external magnetic field (B) and *E. coli* cells and Fe_3O_4@PPy NPs treated with NIR irradiation (C).

As explained before, the adsorption of the positively-charged NPs on the negatively-charged bacteria were boosted by the cationic pyrrole polymer, which easily adsorbed onto the surface of the *E. coli* membrane through electrostatic interactions. Based on this interaction ability, the Fe_3O_4@PPy NPs can be suggested as an adsorbent material for bacteria removal upon application of an external magnetic field. In addition, the prepared adsorbent materials can simultaneously absorb light energy and convert it into thermal energy, hence playing a local heating effect. The photothermal effect of Fe_3O_4@PPy NPs led to an increase of the temperature of bacteria suspensions above the threshold temperature of the bacteria survival. As a consequence, the bacteria membrane was damaged, the intracellular components leaked out, the vital movements were impaired, and the bacteria were eventually inactivated.[35] Under the synergistic action of the adsorption and heat effect, the photothermal sterilization property of Fe_3O_4@PPy NPs was made more effective.

3.6. Recyclability of Fe_3O_4@PPy NPs for photothermal sterilization

The magnetic properties of Fe_3O_4@PPy NPs allowed for their easy separation and

reutilization using an external magnetic field. The recyclability of Fe_3O_4@PPy NPs for photothermal sterilization was determined by inactivation tests mediated by recycled NPs. As shown in **Figure 7A-7B**, over 99% of bacteria were inactivated using recycled Fe_3O_4@PPy NPs for each cycle with the same photothermal procedure. The spectral absorption of the reused Fe_3O_4@PPy NPs also showed no significant variations after four cycles (**Figure 7C**). These results demonstrate the high stability and recyclability of the prepared Fe_3O_4@PPy NPs. Therefore, it can be further confirmed that the Fe_3O_4@PPy NPs can be considered a reliable alternative in the photothermal sterilization of water.

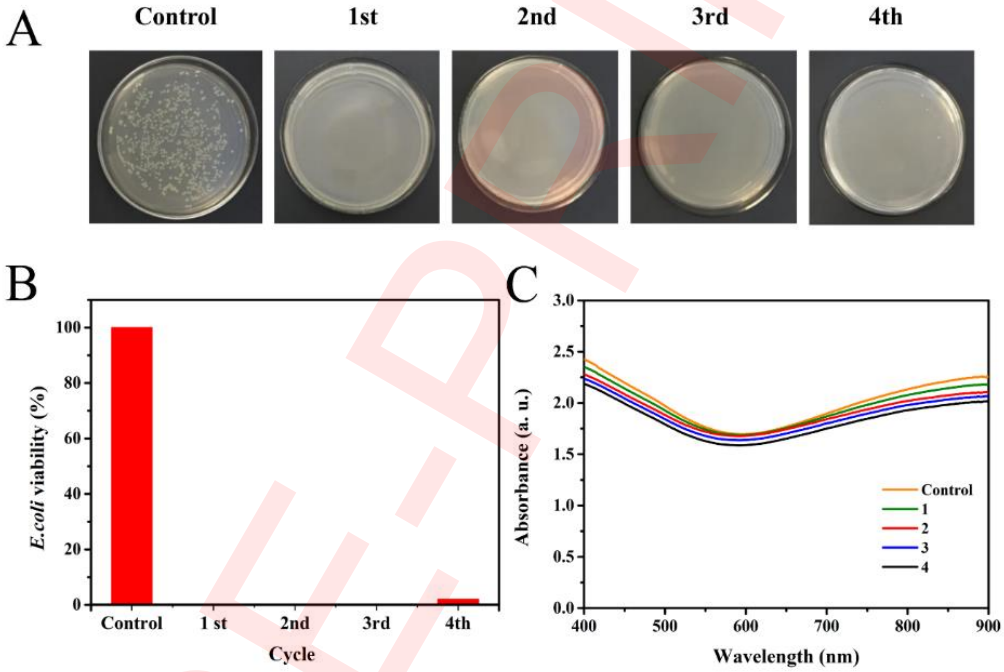

Figure 7. Photographs of survival *E. coli* after photothermal sterilization with recycled (four cycles) Fe_3O_4@PPy NPs (A), *E. coli* viability for each cycle (B) and UV-vis spectra of recycled Fe_3O_4@PPy NPs after NIR irradiation and magnetic separation (C)

4. Conclusions

In this work, we have successfully developed Fe_3O_4@PPy NPs for inactivation of bacteria suspended in aqueous media. The sterilization activity of Fe_3O_4@PPy NPs was tested successfully against *E. coli* in a water system, and was explained in terms of: i) adsorption capability of Fe_3O_4@PPy NPs mediated by electrostatic interaction between NPs and bacteria surface; and ii) high photothermal conversion efficiency of Fe_3O_4@PPy NPs and a local heating effect, due to their strong absorption from UV to NIR regions, thus making possible the conversion of large portion of solar energy to thermal energy, which can lead the bacteria suspension temperature above the threshold of the bacteria survival. In addition, the excellent photothermal stability and recyclability of Fe_3O_4@PPy NPs make them an appealing system for multiple uses without affecting the ultimate photothermal sterilization ability. We believe that the excellent performance of the Fe_3O_4@PPy NPs, based on the dual adsorption behavior and photothermal sterilization property, will provide a new pathway for the water safety management.

Conflicts of interest

There are no conflicts to declare.

Acknowledgements

The authors gratefully acknowledge the financial supports by The National Natural Science Foundation (81901868), the Fundamental Research Funds for the Central Universities (2572018BU03) and the financial support by National Key R&D Program of China (2017YFD0600706).

References

1. Ahuja, S., Global Water Challenges and Solutions. In *Advances in Water Purification Techniques*, Elsevier: 2019; pp 17-39.

2. Chung, H. J.; Reiner, T.; Budin, G.; Min, C.; Liong, M.; Issadore, D.; Lee, H.; Weissleder, R., Ubiquitous detection of gram-positive bacteria with bioorthogonal magnetofluorescent nanoparticles. *ACS nano* **2011,** *5* (11), 8834-8841.

3. (a) He, J.; Wang, W.; Shi, R.; Zhang, W.; Yang, X.; Shi, W.; Cui, F., High speed water purification and efficient phosphate rejection by active nanofibrous membrane for microbial contamination and regrowth control. *Chemical Engineering Journal* **2018,** *337*, 428-435; (b) Lutzer, W., Apparatus and method for thermal sterilization of liquids. Google Patents: 2004; (c) Song, K.; Mohseni, M.; Taghipour, F., Application of ultraviolet light-emitting diodes (UV-LEDs) for water disinfection: A review. *Water research* **2016,** *94*, 341-349.

4. (a) Zhai, H.; Zhang, X.; Zhu, X.; Liu, J.; Ji, M., Formation of brominated disinfection byproducts during chloramination of drinking water: new polar species and overall kinetics. *Environmental science & technology* **2014,** *48* (5), 2579-2588; (b) Glaze, W. H., Drinking-water treatment with ozone. *Environmental science & technology* **1987,** *21* (3), 224-230.

5. (a) Cabello, F. C., Heavy use of prophylactic antibiotics in aquaculture: a growing problem for human and animal health and for the environment. *Environmental Microbiology* **2006,** *8* (7), 1137-1144; (b) Agnihotri, S.; Mukherji, S.; Mukherji, S., Immobilized silver nanoparticles enhance contact killing and show highest efficacy:

elucidation of the mechanism of bactericidal action of silver. *Nanoscale* **2013,** *5* (16), 7328-7340; (c) Li, Q.; Mahendra, S.; Lyon, D. Y.; Brunet, L.; Liga, M. V.; Li, D.; Alvarez, P. J. J., Antimicrobial nanomaterials for water disinfection and microbial control: Potential applications and implications. *Water Research* **2008,** *42* (18), 4591-4602.

6. (a) Permatasari, F. A.; Fukazawa, H.; Ogi, T.; Iskandar, F.; Okuyama, K., Design of pyrrolic-N-rich carbon dots with absorption in the first near-infrared window for photothermal therapy. *ACS Applied Nano Materials* **2018,** *1* (5), 2368-2375; (b) Yang, K.; Xu, H.; Cheng, L.; Sun, C.; Wang, J.; Liu, Z., In Vitro and In Vivo Near-Infrared Photothermal Therapy of Cancer Using Polypyrrole Organic Nanoparticles. *Advanced Materials* **2012,** *24* (41), 5586-5592; (c) Guo, B.; Huang, Z.; Shi, Q.; Middha, E.; Xu, S.; Li, L.; Wu, M.; Jiang, J.; Hu, Q.; Fu, Z., Organic Small Molecule Based Photothermal Agents with Molecular Rotors for Malignant Breast Cancer Therapy. *Advanced Functional Materials* **2020,** *30* (5), 1907093.

7. (a) Roti Roti, J. L., Cellular responses to hyperthermia (40–46 C): Cell killing and molecular events. *International Journal of hyperthermia* **2008,** *24* (1), 3-15; (b) Liu, Y.; Bhattarai, P.; Dai, Z.; Chen, X., Photothermal therapy and photoacoustic imaging via nanotheranostics in fighting cancer. *Chemical Society Reviews* **2019,** *48* (7), 2053-2108.

8. Xu, J.-W.; Yao, K.; Xu, Z.-K., Nanomaterials with a photothermal effect for antibacterial activities: an overview. *Nanoscale* **2019,** *11* (18), 8680-8691.

9. (a) Jiang, T.; He, J.; Sun, L.; Wang, Y.; Li, Z.; Wang, Q.; Sun, Y.; Wang, W.; Yu, M., Highly efficient photothermal sterilization of water mediated by Prussian blue

517 nanocages. *Environmental Science-Nano* **2018,** *5* (5), 1161-1168; (b) Huang, W.-C.;
518 Tsai, P.-J.; Chen, Y.-C., Multifunctional Fe3O4@Au Nanoeggs as Photothermal
519 Agents for Selective Killing of Nosocomial and Antibiotic-Resistant Bacteria. *Small*
520 **2009,** *5* (1), 51-56.
521 10. (a) Jin, Y.; Deng, J.; Yu, J.; Yang, C.; Tong, M.; Hou, Y., Fe5C2 nanoparticles: a
522 reusable bactericidal material with photothermal effects under near-infrared irradiation.
523 *Journal of Materials Chemistry B* **2015,** *3* (19), 3993-4000; (b) Wang, N.; Hu, B.; Chen,
524 M.-L.; Wang, J.-H., Polyethylenimine mediated silver nanoparticle-decorated magnetic
525 graphene as a promising photothermal antibacterial agent. *Nanotechnology* **2015,** *26*
526 (19).
527 11. (a) Chen, H.; Ma, Y.; Wang, X.; Wu, X.; Zha, Z., Facile synthesis of Prussian blue
528 nanoparticles as pH-responsive drug carriers for combined photothermal-chemo
529 treatment of cancer. *Rsc Advances* **2017,** *7* (1), 248-255; (b) Ji, H.; Sun, H.; Qu, X.,
530 Antibacterial applications of graphene-based nanomaterials: Recent achievements and
531 challenges. *Advanced Drug Delivery Reviews* **2016,** *105*, 176-189.
532 12. (a) Zha, Z.; Yue, X.; Ren, Q.; Dai, Z., Uniform Polypyrrole Nanoparticles with
533 High Photothermal Conversion Efficiency for Photothermal Ablation of Cancer Cells.
534 *Advanced Materials* **2013,** *25* (5), 777-782; (b) Qin, G.; Qiu, J., Ordered polypyrrole
535 nanorings with near-infrared spectrum absorption and photothermal conversion
536 performance. *Chemical Engineering Journal* **2019,** *359*, 652-661; (c) Liao, Y.; Wang,
537 X.; Qian, W.; Li, Y.; Li, X.; Yu, D.-G., Bulk synthesis, optimization, and
538 characterization of highly dispersible polypyrrole nanoparticles toward protein

539 separation using nanocomposite membranes. *Journal of colloid and interface science*
540 **2012,** *386* (1), 148-157.
541 13. (a) Pfluger, P.; Street, G., Chemical, electronic, and structural properties of
542 conducting heterocyclic polymers: a view by XPS. *The Journal of chemical physics*
543 **1984,** *80* (1), 544-553; (b) Bjorklund, R. B.; Liedberg, B., Electrically conducting
544 composites of colloidal polypyrrole and methylcellulose. *Journal of the Chemical*
545 *Society, Chemical Communications* **1986,** (16), 1293-1295.
546 14. (a) Xie, L.; Yu, Z.; Islam, S. M.; Shi, K.; Cheng, Y.; Yuan, M.; Zhao, J.; Sun, G.;
547 Li, H.; Ma, S., Remarkable Acid Stability of Polypyrrole-MoS4: A Highly Selective
548 and Efficient Scavenger of Heavy Metals Over a Wide pH Range. *Advanced Functional*
549 *Materials* **2018,** *28* (20), 1800502; (b) Prissanaroon-Ouajai, W.; Pigram, P. J.; Jones,
550 R.; Sirivat, A., A sensitive and highly stable polypyrrole-based pH sensor with
551 hydroquinone monosulfonate and oxalate co-doping. *Sensors and Actuators B:*
552 *Chemical* **2009,** *138* (2), 504-511.
553 15. Wu, K.; Su, D.; Saha, R.; Liu, J.; Chugh, V. K.; Wang, J.-P., Magnetic Particle
554 Spectroscopy: A Short Review of Applications using Magnetic Nanoparticles. *ACS*
555 *Applied Nano Materials* **2020**.
556 16. Ding, H. L.; Zhang, Y. X.; Wang, S.; Xu, J. M.; Xu, S. C.; Li, G. H., Fe3O4@SiO2
557 Core/Shell Nanoparticles: The Silica Coating Regulations with a Single Core for
558 Different Core Sizes and Shell Thicknesses. *Chemistry of Materials* **2012,** *24* (23),
559 4572-4580.

17. (a) Liu, J.; Sun, Z.; Deng, Y.; Zou, Y.; Li, C.; Guo, X.; Xiong, L.; Gao, Y.; Li, F.; Zhao, D., Highly Water-Dispersible Biocompatible Magnetite Particles with Low Cytotoxicity Stabilized by Citrate Groups. *Angewandte Chemie-International Edition* **2009,** *48* (32), 5875-5879; (b) Bonyasi, F.; Hekmati, M.; Veisi, H., Preparation of core/shell nanostructure Fe3O4@ PEG400-SO3H as heterogeneous and magnetically recyclable nanocatalyst for one-pot synthesis of substituted pyrroles by Paal-Knorr reaction at room temperature. *Journal of colloid and interface science* **2017,** *496*, 177-187.

18. Honary, S.; Zahir, F., Effect of Zeta Potential on the Properties of Nano-Drug Delivery Systems - A Review (Part 1). *Tropical Journal of Pharmaceutical Research* **2013,** *12* (2), 255-264.

19. Chang, K.; Liu, Y.; Hu, D.; Qi, Q.; Gao, D.; Wang, Y.; Li, D.; Zhang, X.; Zheng, H.; Sheng, Z., Highly stable conjugated polymer dots as multifunctional agents for photoacoustic imaging-guided photothermal therapy. *ACS applied materials & interfaces* **2018,** *10* (8), 7012-7021.

20. Li, B.; Wang, Q.; Zou, R.; Liu, X.; Xu, K.; Li, W.; Hu, J., Cu 7.2 S 4 nanocrystals: a novel photothermal agent with a 56.7% photothermal conversion efficiency for photothermal therapy of cancer cells. *Nanoscale* **2014,** *6* (6), 3274-3282.

21. Deng, H.; Li, X. L.; Peng, Q.; Wang, X.; Chen, J. P.; Li, Y. D., Monodisperse magnetic single-crystal ferrite microspheres. *Angewandte Chemie-International Edition* **2005,** *44* (18), 2782-2785.

22. Lee, M.-Y.; Park, S.-J.; Park, K.; Kim, K. S.; Lee, H.; Hahn, S. K., Target-Specific Gene Silencing of Layer-by-Layer Assembled Gold-Cysteamine/siRNA/PEI/HA Nanocomplex. *Acs Nano* **2011,** *5* (8), 6138-6147.

23. Lu, X.; Mao, H.; Zhang, W., Fabrication of core-shell Fe3O4/polypyrrole and hollow polypyrrole microspheres. *Polymer Composites* **2009,** *30* (6), 847-854.

24. Zhu, W.; Shen, X.; Zhu, C.; Li, B.; Hong, J.; Zhou, X., Turn-on fluorescent assay based on purification system via magnetic separation for highly sensitive probing of adenosine. *Sensors and Actuators B-Chemical* **2018,** *259*, 855-861.

25. (a) Li, Y.; Chen, G.; Li, Q.; Qiu, G.; Liu, X., Facile synthesis, magnetic and microwave absorption properties of Fe3O4/polypyrrole core/shell nanocomposite. *Journal of Alloys and Compounds* **2011,** *509* (10), 4104-4107; (b) Wang, C.; Yang, M.; Liu, L.; Xu, Y.; Zhang, X.; Cheng, X.; Gao, S.; Gao, Y.; Huo, L., One-step synthesis of polypyrrole/Fe2O3 nanocomposite and the enhanced response of NO2 at low temperature. *Journal of colloid and interface science* **2020,** *560*, 312-320.

26. Dong, H.; Lo, I. M., Influence of humic acid on the colloidal stability of surface-modified nano zero-valent iron. *Water research* **2013,** *47* (1), 419-427.

27. Tian, Q.; Wang, Q.; Yao, K. X.; Teng, B.; Zhang, J.; Yang, S.; Han, Y., Multifunctional Polypyrrole@ Fe3O4 Nanoparticles for Dual-Modal Imaging and In Vivo Photothermal Cancer Therapy. *Small* **2014,** *10* (6), 1063-1068.

28. Gassie, L. W.; Englehardt, J. D., Advanced oxidation and disinfection processes for onsite net-zero greywater reuse: A review. *Water research* **2017,** *125*, 384-399.

29. (a) Hijnen, W.; Suylen, G.; Bahlman, J.; Brouwer-Hanzens, A.; Medema, G., GAC adsorption filters as barriers for viruses, bacteria and protozoan (oo) cysts in water treatment. *Water Research* **2010,** *44* (4), 1224-1234; (b) Smith, S. C.; Rodrigues, D. F., Carbon-based nanomaterials for removal of chemical and biological contaminants from water: a review of mechanisms and applications. *Carbon* **2015,** *91*, 122-143.

30. Yang, J.; Zhang, X.; Ma, Y.-H.; Gao, G.; Chen, X.; Jia, H.-R.; Li, Y.-H.; Chen, Z.; Wu, F.-G., Carbon dot-based platform for simultaneous bacterial distinguishment and antibacterial applications. *ACS applied materials & interfaces* **2016,** *8* (47), 32170-32181.

31. (a) Chen, J.; Andler, S. M.; Goddard, J. M.; Nugen, S. R.; Rotello, V. M., Integrating recognition elements with nanomaterials for bacteria sensing. *Chemical Society Reviews* **2017,** *46* (5), 1272-1283; (b) Zhan, S.; Zhu, D.; Ma, S.; Yu, W.; Jia, Y.; Li, Y.; Yu, H.; Shen, Z., Highly efficient removal of pathogenic bacteria with magnetic graphene composite. *ACS applied materials & interfaces* **2015,** *7* (7), 4290-4298.

32. Busscher, H. J.; Dijkstra, R. J.; Engels, E.; Langworthy, D. E.; Collias, D. I.; Bjorkquist, D. W.; Mitchell, M. D.; van der Mei, H. C., Removal of two waterborne pathogenic bacterial strains by activated carbon particles prior to and after charge modification. *Environmental science & technology* **2006,** *40* (21), 6799-6804.

33. Liang, X.; Li, Y.; Li, X.; Jing, L.; Deng, Z.; Yue, X.; Li, C.; Dai, Z., PEGylated polypyrrole nanoparticles conjugating gadolinium chelates for dual-modal

623 MRI/photoacoustic imaging guided photothermal therapy of cancer. *Advanced*
624 *Functional Materials* **2015,** *25* (9), 1451-1462.
625 34. Wu, M.-C.; Deokar, A. R.; Liao, J.-H.; Shih, P.-Y.; Ling, Y.-C., Graphene-based
626 photothermal agent for rapid and effective killing of bacteria. *ACS nano* **2013,** *7* (2),
627 1281-1290.
628 35. (a) Guo, N.; Zang, Y.-P.; Cui, Q.; Gai, Q.-Y.; Jiao, J.; Wang, W.; Zu, Y.-G.; Fu,
629 Y.-J., The preservative potential of Amomum tsaoko essential oil against E. coil, its
630 antibacterial property and mode of action. *Food Control* **2017,** *75*, 236-245; (b) Li, Z.;
631 Wu, L.; Wang, H.; Zhou, W.; Liu, H.; Cui, H.; Li, P.; Chu, P. K.; Yu, X.-F., Synergistic
632 antibacterial activity of black phosphorus nanosheets modified with titanium
633 aminobenzenesulfanato complexes. *ACS Applied Nano Materials* **2019,** *2* (3), 1202-
634 1209.